J. Fluid Mech. (1998), *vol.* 375, *pp.* 235–263. Printed in the United Kingdom

Direct numerical simulation of turbulence modulation by particles in isotropic turbulence

By MARC BOIVIN[1]†, OLIVIER SIMONIN[1,2] AND KYLE D. SQUIRES[3]

[1]Laboratoire National d'Hydraulique, Electricité de France, 6 Quai Watier, 78400 Chatou, France

[2]Institut de Mecanique des Fluides, Institut National Polytechnique/ENSEEIHT, 31400 Toulouse, France

[3]Mechanical and Aerospace Engineering Department, Arizona State University, Box 876106, Tempe, AZ 85287-6106, USA

(Received 24 January 1997 and in revised form 2 June 1998)

The modulation of isotropic turbulence by particles has been investigated using direct numerical simulation (DNS). The particular focus of the present work is on the class of dilute flows in which particle volume fractions and inter-particle collisions are negligible. Gravitational settling is also neglected and particle motion is assumed to be governed by drag with particle relaxation times ranging from the Kolmogorov scale to the Eulerian time scale of the turbulence and particle mass loadings up to 1. The velocity field was made statistically stationary by forcing the low wavenumbers of the flow. The calculations were performed using 96^3 collocation points and the Taylor-scale Reynolds number for the stationary flow was 62. The effect of particles on the turbulence was included in the Navier–Stokes equations using the point-force approximation in which 96^3 particles were used in the calculations. DNS results show that particles increasingly dissipate fluid kinetic energy with increased loading, with the reduction in kinetic energy being relatively independent of the particle relaxation time. Viscous dissipation in the fluid decreases with increased loading and is larger for particles with smaller relaxation times. Fluid energy spectra show that there is a non-uniform distortion of the turbulence with a relative increase in small-scale energy. The non-uniform distortion significantly affects the transport of the dissipation rate, with the production and destruction of dissipation exhibiting completely different behaviours. The spectrum of the fluid–particle energy exchange rate shows that the fluid drags particles at low wavenumbers while the converse is true at high wavenumbers for small particles. A spectral analysis shows that the increase of the high-wavenumber portion of the fluid energy spectrum can be attributed to transfer of the fluid–particle covariance by the fluid turbulence. This in turn explains the relative increase of small-scale energy caused by small particles observed in the present simulations as well as those of Squires & Eaton (1990) and Elghobashi & Truesdell (1993).

1. Introduction

The interaction of solid particles or liquid droplets with gas-phase turbulent flows controls the performance of many engineering devices and is important in natural

† Present address: IBM, 224, bd John Kennedy, 91105 Corbeil-Essonnes, France.

processes as well. Examples include the combustion of pulverized coal or liquid sprays, transport of particulate solids, gas-phase reactions controlled by particulate catalysts, dust storms, and atmospheric dispersal of pollutants. In each of these areas an increased understanding of the fundamental phenomena that drive the complex interactions between the particle cloud and turbulent carrier flow is needed to ultimately improve the design of engineering devices in which these flows occur.

Within the vast array of applications encompassed by two-phase flows, the particular interest of the present work is on the interaction with a turbulent carrier flow of a dilute dispersed phase of particles with densities substantially larger than the carrier flow, i.e. $\rho_2/\rho_1 \sim O(10^3)$ where ρ_2 and ρ_1 denote particle and fluid density, respectively. For dilute flows the volume fraction of the particles, α_2, is small. However, the particle mass loading, $\phi = \alpha_2\rho_2/\rho_1$, can be large enough such that momentum exchange between particles and fluid results in a significant modulation of the turbulence, typically referred to as two-way coupling (e.g. see Crowe, Troutt & Chung 1996).

For this class of two-phase flows the modulation of turbulence by particles is complex and still not well understood. For example, experimental measurements in shear flows, e.g. particle-laden jets and boundary layers, have shown that turbulence velocity fluctuations may be either increased or decreased due to the modulation of the flow by heavy particles (e.g. see Tsuji, Morikawa & Shiomi 1984; Modarress, Tan & Elghobashi 1984; Shuen *et al.* 1985; Fleckhaus, Hishida & Maeda 1987; Hardalupas, Taylor & Whitelaw 1989; Gore & Crowe 1989; Rogers & Eaton 1991; Kulick, Fessler & Eaton 1994). In turbulent shear flows it is often difficult to separate the direct modulation of the turbulence due to momentum exchange with particles from the indirect changes occurring through modification of turbulence production mechanisms via interactions with mean gradients. Furthermore, it is usually difficult in experiments to isolate the effects of different parameters on measurements.

Numerical simulation offers another approach for examining the interactions between particles and turbulence and the modulation of turbulence by particles. For particle-laden flows traditional approaches relying on solution of the Reynolds-averaged Navier–Stokes equations require empirical input, principally the prescription of turbulence properties along particle trajectories. For applications of one-way coupling, i.e. no modulation of the flow, various modelling approaches have been developed which adequately describe dispersion in simple flows, though the central problem of prescribing Lagrangian quantities along particle trajectories remains an open question (e.g. see Simonin, Deutsch & Minier 1993; Simonin, Deutsch & Boivin 1995). For applications of turbulence modulation by particles, turbulence quantities such as the kinetic energy and dissipation rate are modified directly by the particles (e.g. through the appearance of source terms in the transport equations) as well as indirectly through changes which particles cause in turbulence dynamics (e.g. see Squires & Eaton 1994). Thus, the empirical input required for Reynolds-averaged approaches at the present time makes it difficult to obtain a fundamental understanding of turbulence modulation.

The most sophisticated numerical approach for examining particle–turbulence interactions is direct numerical simulation (DNS). In DNS the Navier–Stokes equations are solved without resorting to *ad hoc* modeling at any scale of motion. The primary advantage for calculation of particle-laden flows is that turbulence properties along particle trajectories are directly available. For applications of one-way coupling several studies have examined heavy particle transport in isotropic turbulence (e.g. see Deutsch & Simonin 1991; Squires & Eaton 1991*a*; Elghobashi & Truesdell 1993; Wang & Maxey 1993).

For two-way coupling DNS has been applied to particle-laden isotropic turbulence and has demonstrated that the distortion of the turbulence is not uniform and is dependent upon the particle relaxation time (e.g. see Squires & Eaton 1990; Elghobashi & Truesdell 1993). Squires & Eaton (1990) considered particle motion in the Stokes regime in which gravitational settling was neglected. Computations were performed using both 32^3 and 64^3 grids at Taylor-scale Reynolds numbers of 35 in which a steady, non-uniform body force was added to the governing equations in order to achieve a statistically stationary flow. Particle sample sizes up to 10^6 were used in the simulations. Mass loadings from zero (one-way coupling) to unity were considered for a series of particle relaxation times varying from $0.3\tau_k$ to $11\tau_k$ where τ_k is the Kolmogorov time scale. For a Stokes drag law without gravitational settling it is straightforward to show that particles will globally dissipate turbulence energy. Squires & Eaton (1990) found that the overall reduction in turbulence kinetic energy for increasing mass loading was insensitive to the particle relaxation time. They also showed a strong preferential concentration of particles into regions of low vorticity and/or high strain rate (see also Wang & Maxey 1993). For cases of turbulence modulation, Squires & Eaton (1994) attributed the non-uniform distortion of the turbulence energy spectrum by particles to preferential concentration.

Elghobashi & Truesdell (1993) examined turbulence modulation by particles in decaying isotropic turbulence using resolutions of 96^3 for the Navier–Stokes equations and 34^3 particles. Particle motion in Elghobashi & Truesdell (1993) was governed by the equation derived by Maxey & Riley (1983). They found that for the large density ratios considered in their simulations particle motion was influenced mostly by drag and gravity. Elghobashi & Truesdell (1993) found that the coupling between particles and fluid resulted in an increase in small-scale energy. The relative increase in the energy of the high-wavenumber components of the velocity field resulted in a larger turbulence dissipation rate. They also found that the effect of gravity resulted in an anisotropic modulation of the turbulence and an enhancement of turbulence energy levels in the direction aligned with gravity. Furthermore, in the directions orthogonal to the gravity vector a reverse cascade of energy from small to large scales was observed.

While the work of Squires & Eaton (1990) and Elghobashi & Truesdell (1993) has advanced our understanding, the effect of turbulence modulation by particles is not fully resolved. For example, in the transport equation for turbulence kinetic energy the coupling between particles and turbulence yields an additional term which accounts for the energy transfer imparted from the particles to the fluid. Both Squires & Eaton (1990) and Elghobashi & Truesdell (1993) have shown that the distortion of the turbulence energy spectrum is sensitive to quantities such as the particle relaxation time. This implies that the energy transfer from particles to turbulence acts non-uniformly across the spectrum. However, neither its overall behaviour, nor its spectral distribution, is available from previous investigations. Both the global value as well as spectral distribution are important not only for increasing fundamental understanding but also for development of engineering models. Relevant in this regard is the work of Baw & Peskin (1971) who have previously considered the spectral modulation of turbulence by particles. They showed that the effect of particles is to decrease the energy at high wavenumbers more than that at low wavenumbers. Their analysis, however, contradicts the results of both Squires & Eaton (1990) and Elghobashi & Truesdell (1993).

The objectives of the present work are to investigate turbulence modulation by particles in isotropic turbulence. In isotropic turbulence there is no production and therefore from a given initial condition, the flow decays over time, i.e. turbulence time

and length scales increase. In decaying turbulence the evolution of quantities such as the kinetic energy and dissipation rate exhibit a dependence on initial conditions. The decay of the flow and dependence on initial conditions complicates interpretation and analysis of both particle motion and turbulence modulation. An alternative to simulation of decaying turbulence is calculation of flows made statistically stationary through an addition of a body force to the Navier–Stokes equations in which the force is added to the low-wavenumber components of the velocity field. Statistically stationary flows can be advanced to an equilibrium in which particle motion, and the effect of particles on the flow, are independent of initial conditions. Time and length scale ratios of the turbulence relative to the particles are also stationary. The forcing scheme used in this work is that developed by Eswaran & Pope (1988), who have shown that the small scales of the velocity field are insensitive to the energy input from the forcing. Discussion of computation of two-way coupling in DNS is presented in §2. The point-force approximation is used in this work to account for momentum transfer between particles and turbulence and important issues relevant to this approach are discussed. An overview of the simulations is also presented in §2 with evolution of statistical quantities and the spectral analysis in §3. A summary of the work may be found in §4.

2. Simulation overview

2.1. *True direct numerical simulation of two-phase flows*

True direct numerical simulations of fluid flows loaded with heavy particles require that one resolves the standard Navier–Stokes equations for the fluid:

$$\frac{\partial u_{1,i}}{\partial x_i} = 0, \tag{2.1}$$

$$\frac{\partial u_{1,i}}{\partial t} + u_{1,k}\frac{\partial u_{1,i}}{\partial x_k} = -\frac{1}{\rho_1}\frac{\partial p_1}{\partial x_i} + \nu_1 \frac{\partial^2 u_{1,i}}{\partial x_k \partial x_k}. \tag{2.2}$$

The effect of the particles on the fluid is formally taken into account through the boundary conditions on the surface of each particle,

$$u_{1,i}(\boldsymbol{x}, t) = w_i^n(\boldsymbol{x}, t) \text{ for all points on the particle surface, i.e. } (\boldsymbol{x}, t) \in \Omega^n, \tag{2.3}$$

where w_i^n is the instantaneous velocity of the surface of particle n (the n superscript is used throughout this work to denote properties of a single particle). For rigid particles in translation, w_i^n is the same everywhere on Ω^n and is equal to the velocity $u_{2,i}^n$ at the centre of the particle. The subscripts 1 and 2 denote the fluid and particle phases, respectively. Thus, in (2.1) and (2.2), $u_{1,i}$ is the ith component of the fluid velocity, p_1 the fluid pressure, and ρ_1 and ν_1 the fluid density and kinematic viscosity, respectively.

Simultaneously to the solution of (2.1)–(2.3), particle trajectories are computed using Lagrangian tracking, the force acting on the particle being computed by direct integration of the simulated fluid stress on the particle surface:

$$\frac{\mathrm{d}x_{2,i}^n}{\mathrm{d}t} = u_{2,i}^n, \tag{2.4}$$

$$\rho_2 \frac{\mathrm{d}u_{2,i}^n}{\mathrm{d}t} = \rho_2 g_i + \int_{\Omega^n} \left[-p_1 \delta_{ij} + \nu_1 \frac{\partial u_{1,i}}{\partial x_j} \right] n_j \, \mathrm{d}\omega. \tag{2.5}$$

The displacement of particle n is $x_{2,i}^n$, the particle density is ρ_2. The outward pointing normal to the surface Ω^n is n_j, and g_i is the acceleration due to gravity. The approach

outlined in (2.1)–(2.5) requires that the velocity field around each particle be accurately resolved and is viable only for calculations with $O(10)$ particles (e.g. see Unverdi & Tryggvason 1992). In a turbulent flow with a large ensemble of particles having diameters on the order of the Kolmogorov length scale this approach is not feasible owing to its enormous computational cost. Thus, approximations are required in order to account for the effect of particle momentum exchange on the flow.

2.2. *Point-force approximation*

Saffman (1973) showed that the perturbation in the fluid due to the presence of a particle decays as the sum of two contributions, one as $1/r$ (long-range) and the other as $1/r^3$ (short-range). For particles small relative to the smallest length scales of the flow, and for particles separated by a distance L large compared to their diameter d, the most important interactions are long-range (e.g. see Koch 1990). Neglecting short-range interactions, e.g. particle wakes, is justifiable for particles with diameters smaller than the Kolmogorov length scale of the flow field undisturbed by the presence of the particle since in that case short-range perturbations are dissipated by viscosity. The focus of this work will be on larger scales in which long-range interactions are dominant. The Navier–Stokes equations can then be written for the fluid everywhere in the domain with the influence of particles taken into account by Dirac distributions of the force, $f^n_{d,i}$, applied to the fluid by each particle,

$$\frac{\partial u_{1,i}}{\partial x_i} = 0, \tag{2.6}$$

$$\frac{\partial u_{1,i}}{\partial t} + u_{1,k}\frac{\partial u_{1,i}}{\partial x_k} = -\frac{1}{\rho_1}\frac{\partial p_1}{\partial x_i} + \nu_1\frac{\partial^2 u_{1,i}}{\partial x_k \partial x_k} + \frac{1}{\rho_1} f_{c,i}, \tag{2.7}$$

where

$$\frac{1}{\rho_1} f_{c,i} = \frac{1}{\rho_1} f^n_{d,i}(x^n_{2,i})\delta(x_i - x^n_{2,i}). \tag{2.8}$$

The force $f^n_{d,i}$ is the opposite of that applied to particle n by the fluid. As shown by Gatignol (1983) and Maxey & Riley (1983), the forces acting on a particle can be considered to arise from three contributions. The first contribution, $\boldsymbol{f}_a$, represents the virtual force that would apply on a fluid element that coincides with the particle position, i.e. pressure forces and viscous stresses. The second contribution, $\boldsymbol{f}_b$, arises from the perturbation of the fluid flow due to the presence of the particle. For a rigid sphere of diameter d in translation, this perturbation of the surrounding unsteady non-uniform flow results in the drag, added mass, and Basset history forces. The third contribution is gravitational settling. For spheres with density ρ_2 large compared to the fluid density ρ_1, $\boldsymbol{f}_b \gg \boldsymbol{f}_a$ and reduces to the drag force. The particle equation of motion can then be written for a single particle n as

$$\frac{\mathrm{d}x^n_{2,i}}{\mathrm{d}t} = u^n_{2,i}, \tag{2.9}$$

$$\rho_2\frac{\mathrm{d}u^n_{2,i}}{\mathrm{d}t} = -f^n_{d,i} + \rho_2 g_i = -\tfrac{3}{4}\rho_1\frac{C^n_D}{d} \mid \boldsymbol{v}^n_r \mid v^n_{r,i} + \rho_2 g_i = -\rho_2\frac{u^n_{2,i} - \tilde{u}^n_{1,i}}{\tau^n_p} + \rho_2 g_i. \tag{2.10}$$

The local drag coefficient in (2.10) is C^n_D and may be expressed in terms of the particle Reynolds number Re^n_p as (Clift, Grace & Weber 1978)

$$C^n_D = \frac{24}{Re^n_p}\left[1 + 0.15 Re_p^{n^{0.687}}\right], \qquad Re^n_p = \frac{\mid \boldsymbol{v}^n_r \mid d}{\nu_1} \leqslant 800, \tag{2.11}$$

where τ_p^n is the particle relaxation time, or time constant, defined as

$$\tau_p^n = \frac{4}{3}\frac{\rho_2}{\rho_1}\frac{C_D^n}{d}|\boldsymbol{v}_r^n| = \frac{d^2}{18\nu_1}\frac{\rho_2}{\rho_1}\ \frac{1}{1+0.15Re_p^{n\,0.687}}\,. \tag{2.12}$$

The local instantaneous relative velocity between particle n and the surrounding fluid is $v_{r,i}^n = u_{2,i}^n - \tilde{u}_{1,i}^n$, where $\tilde{u}_{1,i}^n$ is the fluid velocity at the position of particle n of the flow field locally undisturbed by the presence of the particle (Gatignol 1983; Maxey & Riley 1983). The expression for the drag force as written above is applicable to particles having diameters smaller than the Kolmogorov length scale, i.e. $d \ll \eta$. If d is comparable to η, Faxén terms should be taken into account (Gatignol 1983; Maxey & Riley 1983). Gravitational settling results in the crossing trajectories effect which strongly influences particle dispersion (Csanady 1963; Squires & Eaton 1991*b*). Elghobashi & Truesdell (1993) have shown that in two-way coupling gravity complicates turbulence modulation. In the current study the parameters varied are particle relaxation time and mass loading; the effect of gravity is not examined. Finally, it should also be noted that for the sake of improving fundamental understanding of two-way coupling within a manageable parameter range, the effect of shear-induced lift has also been neglected. Shear-induced lift may influence particle motion in certain regimes, which could in turn alter the mechanisms of turbulence modulation considered in this work.

For a flow containing N_p particles, the fluid velocity $\tilde{u}_{1,i}^n$ required in (2.10) is that locally undisturbed by the presence of particle n, but taking into account the disturbances created by all other $(N_p - 1)$ particles in the flow. This in turn requires that to determine the motion of each particle, a total of N_p flow fields is required. Only in the limit of one-way coupling is $\tilde{u}_{1,i}^n$ identical to that in a single-phase turbulent flow.

2.3. *Effective direct numerical simulation of two-phase flows*

One approach to obtaining the locally undisturbed fluid velocities $\tilde{u}_{1,i}^n$ would be to resolve the flow field $u_{1,i}$ influenced by the entire ensemble of particles and then subtract the local perturbation induced by the particle presence. Considering Stokes flows in the dilute regime, i.e. inter-particle separations large with respect to the particle diameter, Saffman (1973) showed that $u_{1,i}$ is the sum of $\tilde{u}_{1,i}^n$ and the local perturbation, the so-called Stokeslet,

$$u_{1,i} = \tilde{u}_{1,i}^n + \frac{3d}{4r}\left[v_{r,i}^n + v_{r,j}^n\frac{r_i r_j}{r^2}\right] \text{ with } r = \mid \boldsymbol{x} - \boldsymbol{x}_2^n \mid, \boldsymbol{r} = \boldsymbol{x} - \boldsymbol{x}_2^n. \tag{2.13}$$

To obtain the locally undisturbed velocity field for each particle, $\tilde{u}_{1,i}^n$, an iteration procedure could be developed using (2.13). For a flow with a large number of particles, however, the computational cost becomes prohibitively large.

For practical purposes with a large sample of particles N_p, and for intermediate particle Reynolds numbers, it is necessary to assume that for each particle, the locally undisturbed fluid velocity field $\tilde{u}_{1,i}^n$ can be approximated by $u_{1,i}$. Therefore, the coupling force $f_{d,i}^n$ may be expressed as

$$f_{d,i}^n = \rho_2\frac{u_{2,i}^n - \tilde{u}_{1,i}^n}{\tau_p^n} \approx \rho_2\frac{u_{2,i}^n - u_{1,i}}{\tau_p^n}. \tag{2.14}$$

An estimate of the error made in simulations in which the approximation (2.14) is

employed can be obtained using (2.13). Defining $\Delta u^n_{1,i}$ as the error, (2.13) shows that

$$\Delta u^n_{1,i} = \tilde{u}^n_{1,i} - u_{1,i} = -\frac{3d}{4r}\left[v^n_{r,i} + v^n_{r,j}\frac{r_i r_j}{r^2}\right]. \tag{2.15}$$

In actual computations, the distance r between particle n and the grid nodes (where the locally undisturbed fluid velocity, $\tilde{u}^n_{1,i}$, is approximated by that from the DNS, $u_{1,i}$) is of the order of the mesh size. Thus, on average, the relative error resulting from the use of (2.14) is $O(d/\Delta x)$ and, in addition to the restriction $d \ll \eta$ imposed by the point-force approximation and neglect of the Faxén contributions in the particle equation of motion, the condition imposed by the approximation of the locally undisturbed velocity $\tilde{u}^n_{1,i}$ by $u_{1,i}$ requires that $d \ll \Delta x$. These constraints are compatible since in a DNS calculation, η is of the order of Δx.

2.4. *Direct numerical simulation of isotropic turbulence*

The method used to obtain the fluid velocity is based on the direct numerical simulation technique developed by Rogallo (1981) in which dependent variables are expanded in Fourier series and the flow is represented in a cubic domain of volume $L^3_{box} = (2\pi)^3$ with periodic boundary conditions. Exact integration of the viscous terms is performed using an integrating factor and the nonlinear terms are calculated in physical space. The discretized equations are time advanced using a second-order Runge–Kutta scheme. The reader is referred to Rogallo (1981) for further details on the method.

The method is applied to computation of homogeneous isotropic turbulence. Isotropic turbulence is non-stationary since in the absence of a production mechanism turbulence decays. As discussed in §1, the continual evolution of turbulence quantities complicates analysis and interpretation of decaying turbulence. Lack of a statistically stationary flow in particle-laden turbulence is even more complex since the ratio of the particle relaxation time to fluid time scales changes as the flow evolves. To alleviate these complications, a spatially non-uniform, time-dependent body force (or acceleration) was added to the low-wavenumber components of the velocity field to maintain a statistically stationary flow.

The large scales were forced using the scheme developed by Eswaran & Pope (1988) and Yeung & Pope (1989) and is based on an Uhlenbeck–Ornstein stochastic process that determines an acceleration for each of the three velocity components and for each non-nul wavenumber mode within a shell in spectral space of radius K_F. The complex-valued body force is added to the momentum equations at each time step. The evolution of one component of the body force f at time level $n+1$ is obtained via

$$f_{n+1} = f_n(1 - \mathrm{d}t/T_F) + e(2\sigma^2 \mathrm{d}t/T_F)^{1/2}, \tag{2.16}$$

where e is a random number taken from a Gaussian distribution of zero mean and unit variance. The characteristic time of the process, T_F, and the forcing variance, σ, were equal to 1.4 and 0.033, respectively. A simple modification of the forcing was adopted in this study since the Uhlenbeck–Ornstein process assumes that the time step dt remains small with respect to the characteristic time of the energetic turbulent structures, i.e. with respect to the Eulerian time scale τ_e (defined using the Eulerian fluid velocity and longitudinal integral length scale, L_e). It is also assumed that the time step dt remains large with respect to the small-scale motion, characterized by the Kolmogorov time scale τ_k, which ensures that the forcing is independent of small-scale motions (Eswaran & Pope 1988). Therefore, the forcing acceleration was

ν_1	q_1^2	ε_1	L_f^e/L_g^e	L_f^e/L_{box}	Re_λ	$k_{max}\eta$	τ_e	τ^ε	τ_1^t	τ_λ	τ_k
0.015	7.00	5.70	1.98	0.148	62	1.26	0.43	1.23	0.35	0.32	0.051

TABLE 1. Flow field parameters

maintained constant over $2\tau_k$ with a ratio $\tau_e/\tau_k \approx 10$. This small modification of the forcing scheme requires longer averaging periods in order to ensure isotropy of the turbulence.

For the simulations reported in this paper the turbulence was resolved using 96^3 collocation points with a forcing radius K_F equal to 8. This resolution provides an adequate separation between the forced modes and small scales and a large enough Reynolds number to obtain a separation between the peak of the energy and dissipation spectra (Yeung & Pope 1989; Boivin 1996). The maximum wavenumber of the simulation k_{max} is $\sqrt{2}/3N$ with N the number of grid points in each direction (Rogallo 1981). As shown by several investigators, values of $k_{max}\eta$ greater than one ensure accurate resolution of small statistics as well as accurate interpolation of fluid velocities (e.g. see Eswaran & Pope 1988; Balachandar & Maxey 1989). The Courant number of the computations was 0.5 in order to minimize time-stepping errors and ensure accurate resolution of the small scales (see Eswaran & Pope 1988 and Yeung & Pope 1988 for further discussion).

Table 1 summarizes the main characteristics of the reference fluid flow, i.e. without influence of the particles on the turbulence, that was obtained following a time development required for the flow to become independent of its initial conditions. The statistics were accumulated over a period of roughly $7\tau_e$. In table 1, q_1^2 and ε_1 are the fluid kinetic energy and dissipation rate, respectively, and are used to form the Eulerian time macro-scale, $\tau^\varepsilon = q_1^2/\varepsilon_1$. The Reynolds number, Re_λ, is based on the Taylor micro-scale λ, defined as

$$q_1^2 = \tfrac{1}{2}\langle u'_{1,i}u'_{1,i}\rangle_1 = \tfrac{3}{2}\langle u_1'^2\rangle_1, \quad \lambda = \left(\frac{15\nu_1\langle u_1'^2\rangle_1}{\varepsilon_1}\right)^{1/2}, \quad Re_\lambda = \lambda\frac{(\langle u_1'^2\rangle_1)^{1/2}}{\nu_1} \tag{2.17}$$

(the $'$ superscript denotes a fluctuating quantity obtained by subtraction of the mean). The kinetic energy and dissipation rate are related to the energy spectrum as

$$q_1^2 = \int_0^\infty E(k)\mathrm{d}k, \quad \varepsilon_1 = \int_0^\infty D(k)\mathrm{d}k = 2\nu_1\int_0^\infty k^2E(k)\mathrm{d}k. \tag{2.18}$$

The Lagrangian integral time scale shown in table 1, τ_1^t, is obtained from integration of the Lagrangian autocorrelation. The Kolmogorov time scale is denoted $\tau_k = (\nu_1/\varepsilon_1)^{1/2}$. Averages of turbulence quantities obtained over the computational volume are denoted $\langle\cdot\rangle_1$. With a ratio L_f^e/L_{box} around 0.15, the computational domain contains an adequate sample of energy-containing eddies to avoid problems due to imposition of periodic boundary conditions (Yeung & Pope 1989). Moreover, the ratio of the longitudinal length scale, L_f^e, to the transverse length scale, L_g^e, is close to 2, in agreement with isotropic relations. Finally, also shown in the table is τ_λ, the time scale representative of the Taylor length scale λ. It is formally defined with the time scale relation at wavenumber $k = 1/\lambda$ valid in the inertial subrange, $\tau_\lambda = (\lambda^2/\varepsilon_1)^{1/3}$ (Hinze 1975).

The energy spectrum for the reference flow is plotted in figure 1. The energy at low wavenumbers differs from that measured in the grid-turbulence experiment of Comte-

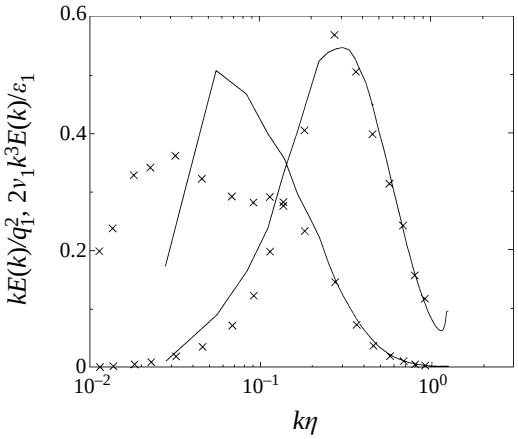

FIGURE 1. Normalized turbulence energy and dissipation spectra of the reference fluid field, $\phi = 0$. ———, DNS; ×, Comte-Bellot & Corrsin (1971).

Bellot & Corrsin (1971). The experimental values are the measurements using a 2 in. grid at a location where $Re_\lambda = 65$, close to $Re_\lambda = 62$ of the reference flow in the DNS. The energy at high wavenumbers follows remarkably well the experimental data, which, considering the comprehensive study of Eswaran & Pope (1988), illustrates that the forcing does not adversely affect the small-scale motion (see Boivin 1996 for further discussion).

2.5. *Numerical implementation of the coupling force*

Properties of the particle cloud were obtained by solving (2.9) and (2.10) for a large ensemble of particles. A second-order Runge–Kutta scheme was used for advancement of the particle velocity and displacement. Interpolation of fluid velocities to particle positions was performed using third-order Lagrange polynomials. Numerical experiments have shown that the scheme is accurate for interpolation of quantities such as the fluid velocity (e.g. see Yeung & Pope 1988; Balachandar & Maxey 1989; Boivin 1996).

Two schemes to incorporate the coupling force in the fluid momentum equations were considered. This process is a projection of the coupling force, defined at the particle position, onto the grid. The first scheme, the so-called Particle-in-Cell (PIC) method, represents the coupling force $f_{c,i}$ as proportional to the accumulation of forces $f_{d,i}^n$ (equation (2.14)) induced by each particle n surrounding a node P (with volume $V = (L_{box}/N)^3$) on which the fluid velocity is calculated (e.g. see Crowe 1982):

$$V f_{c,i}^{P(x,y,z)} = \alpha \sum_{n\ in\ V} f_{d,i}^n, \tag{2.19}$$

where α is a constant of proportionality to be defined. In the second scheme, rather than a summation of $f_{d,i}^n$ around a node P, the force exerted by each particle on the fluid is projected onto the grid

$$V f_{c,i}^{P(x,y,z)} = \alpha \sum_{n\ in\ V} \mathrm{proj}(f_{d,i}^n, P(x,y,z)). \tag{2.20}$$

The weights in the projection operation in (2.20) can be based on the cell volumes as in Squires & Eaton (1990) or on the distances between particle n and the eight

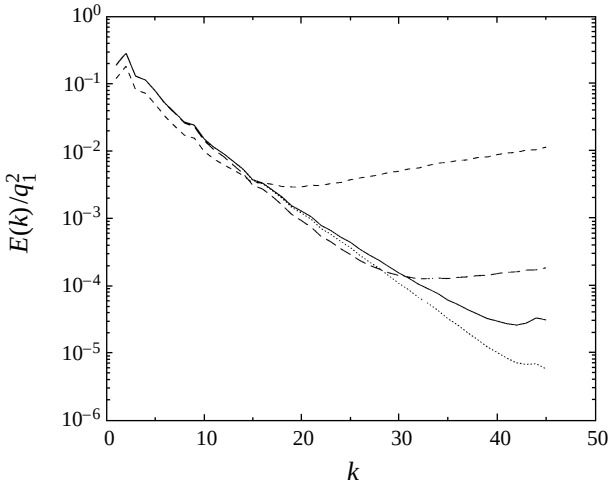

FIGURE 2. Turbulence energy spectrum from one realization of a statistically stationary flow at zero mass loading: ———, spectrum before interpolation; ·····, after interpolation on to a mesh shifted half a grid cell; – – – –, after interpolation on to 96^3 random particle locations and projection back on to the grid using the PIC method (2.19); — — —, after interpolation on to 96^3 random particle locations and projection back on to the grid using linear projection (2.20).

nearest grid nodes as employed by Elghobashi & Truesdell (1993). Both approaches yield similar results (Boivin 1996); therefore, only the results in which the weights are based on cell volumes are presented below. The reader is referred to the recent works by Sundaram & Collins (1996) and Maxey, Patel & Wang (1997) for further discussion of other options for implementation of the coupling force.

The two schemes (2.19) and (2.20) were tested using an instantaneous fluid velocity field which was interpolated to 96^3 random particle locations within the computational box using third-order Lagrange polynomials. Fluid velocities obtained from the interpolation step were then projected back onto the grid using (2.19) and (2.20). Figure 2 shows the energy spectra of the fluid velocities resulting from this procedure. The second method (2.20) recovers much more of the kinetic energy following the interpolation and projection steps as compared with the PIC scheme, e.g. a decrease in the initial kinetic energy of only 2% using (2.20) compared to a reduction of 38% when using (2.19). The figure also shows that the high-wavenumber end of the energy spectrum is more accurately recovered using (2.20) compared to the PIC scheme. Also shown in figure 2 is the energy spectrum of the fluid velocities following interpolation of the initial field onto a mesh shifted by half a grid cell (dotted curve in the figure). This curve shows that there is a relatively small filtering of high-wavenumber components of the velocity field due to interpolation. Comparison of this spectrum with those obtained following the projection steps shows the error resulting from the projection schemes. It is also important to note that another factor influencing the errors resulting from interpolation and projection is the particle sample size. A smaller ensemble of particles will result in a larger error in both the interpolation and projection steps. The simulations presented in §3 were performed using the same number of particles, 96^3, as in the tests outlined in figure 2.

The constant of proportionality α in (2.19) and (2.20) depends on the nature of the particles, i.e. actual particles in which each particle in the simulation represents a physical particle, or stochastic particles in which each particle represents the effect

$(\tau_{12}^F)_{Stokes}$	0.069	0.260	0.696
$d/\eta_{\phi=0}$	0.11	0.21	0.35
$Re_p(\phi = 0)$	0.38	0.84	1.52
$\tau_{12}^F(\phi = 0)$	0.064	0.230	0.580
$\tau_{12}^F/\tau_k(\phi = 0)$	1.26	4.49	11.38
$\tau_e/\tau_{12}^F(\phi = 0)$	6.68	1.88	0.74

TABLE 2. Particle characteristics at zero mass loading.

of several. Squires & Eaton (1990) and Elghobashi & Truesdell (1993) considered stochastic particles. In that case, it means that for a given particle relaxation time and mass loading, the influence of the particles on the fluid motion is assumed to be independent of the average distance L between particles. This is fully legitimate when L is small with respect to the smallest fluid length scale, the Kolmogorov scale η. For actual particles $\alpha = \pi d^3/6$, i.e. the volume of a single particle, while for stochastic particles $\alpha = \alpha_2/N_p$ where α_2 is the volume fraction of the dispersed phase. For actual particles the volume fraction α_2 is determined from the total number of particles in the simulation, $\alpha_2 = N_p\pi d^3/6/L_{box}^3$, while for stochastic particles, α_2 is set arbitrarily through the specification of the mass loading $\phi = \alpha_2\rho_2/\rho_1$. It should be noted that the condition $L \ll \eta$ required for correspondence between stochastic and actual particles is not met in the previous calculations of two-way coupling by Squires & Eaton (1990) and Elghobashi & Truesdell (1993), nor in the present simulations. Thus, the particle relaxation time should be considered a parameter of the simulation, along with the number density, which is determined based on numerical considerations as shown in figure 2. The mass loading is then changed by varying the material density of the particles.

2.6. *Particle parameters and simulation validation*

The particle parameters are summarized in table 2. The Stokes relaxation time is denoted $(\tau_{12}^F)_{Stokes}$, τ_{12}^F is the particle relaxation time obtained from an ensemble and time average over all particles with the same material properties. Simulations were performed for three particle relaxation times and a series of mass loadings ϕ varying from zero (one-way coupling) to unity. Since corrections are incorporated for nonlinear drag via C_D, the particle diameter d and density relative to the fluid, ρ_2/ρ_1 (or, equivalently, the relaxation time and density ratio) must be specified. The particle relaxation times were chosen roughly equal to the Kolmogorov, Taylor, and Eulerian integral time scales, $\tau_{k,\phi=0}$, $\tau_{\lambda,\phi=0}$ and $\tau_{e,\phi=0}$, of the reference flow at zero mass loading. The corresponding diameter variation yields particle Reynolds numbers up to approximately 1.5 for the largest particles.

As discussed in §2.3, the fluid velocity locally undisturbed by the particle presence is approximated in the DNS by the fluid velocity perturbed by all particles. While this is an approximation required in order to simulate two-way coupling with many particles, interpolation of fluid velocities to particle positions and projection of the coupling force onto the grid smooths the disturbance created by a particle on its own motion. Higher-order-accurate interpolation will also, in general, decrease the weight in the interpolation of the velocity disturbance created by a particle. In addition, the influence of the disturbance created by any particle on self-induced motion is lessened by increasing the sample size. Using a linear projection to the eight nearest grid points surrounding the particle implies that each grid node incorporates the

disturbance from approximately $8\langle p\rangle$ particles where $\langle p\rangle$ is the average number of particles per cell. Thus, on average, $1/8/\langle p\rangle$ of the velocity disturbance interpolated back to the particle is created by the particle itself, the complement to 1 results from perturbations created by other particles.

An estimate of the approximation of the locally undisturbed fluid velocity $\tilde{u}^n_{1,i}$ in (2.10) by $u_{1,i}$, which is modified by all particles and computed in DNS, was examined through calculation of the position and velocity of two groups of particles having the same material properties in the same simulation. Only the particles of the first group influenced the fluid flow. For both groups the drag force was computed with the resolved $u_{1,i}$ which is, by construction, an approximation of $\tilde{u}^n_{1,i}$ for the particles of the first group but the exact $\tilde{u}^n_{1,i}$ for the second group. Statistics from both groups such as the particle kinetic energy, the fluid–particle velocity covariance, the fluid kinetic energy along particle trajectories, and the fluid–particle energy exchange rate in the fluid kinetic energy equation differed by less than 1%.

3. Results

The simulations were started from an arbitrary initial condition that was time advanced until the rate of energy added to the flow through the forcing balanced the dissipation. Particles were then placed randomly throughout the computational domain with an initial velocity identical to the fluid velocity at the particle location. Periodic boundary conditions enforced in solution of the governing equations for the fluid ensure that the particle number density field is statistically homogeneous. Particles were tracked for an additional development period of roughly four relaxation times in order for the particle cloud to reach its own equilibrium condition. Only from that point were statistics accumulated by advancing the simulations an additional seven large-scale time periods τ_e. Around six eddy-turnover times were necessary to reach a new equilibrium in which production was balanced by both viscous dissipation in the fluid and drag. Statistics were then obtained for an additional $7\tau_e$.

3.1. *Fluid-phase statistics*

3.1.1. *Effect of particles on turbulence statistics*

The equilibrium values of the turbulence kinetic energy, q_1^2, and viscous dissipation rate, ε_1, in the fluid are shown in figures 3 and 4, respectively. In the absence of gravitational settling small particles, $d \ll \eta$, will dissipate turbulence kinetic energy, consistent with the results in figure 3. The results in both figure 3 and figure 4 are also in good agreement with Squires & Eaton (1990). Fluid turbulence energy spectra $E(k)$ are shown in figure 5. For larger mass loading the energy at low wavenumbers is diminished independent of τ^F_{12}, while particles can enhance the high-wavenumber components, the behaviour at high k depending on ϕ and τ^F_{12}. This is consistent with the different behaviour exhibited by q_1^2 and ε_1 in figures 3 and 4. For the larger particles and increasing ϕ, small-scale energy reaches a minimum that occurs at lower mass loading that decreases with τ^F_{12}. Note that for $\tau^F_{12} = 0.064$ a net production of small-scale energy occurs at larger ϕ, similar to that observed by Squires & Eaton (1990). Thus, in general, there is a similar effect on the lower wavenumbers of the fluid turbulence by both the smaller and larger particles. At the higher wavenumbers, the turbulence spectral density is attenuated by the larger particles, and increased by the smaller particles. These results are contradictory to the notion that particles attenuate, on average, structures having a time scale smaller than their relaxation

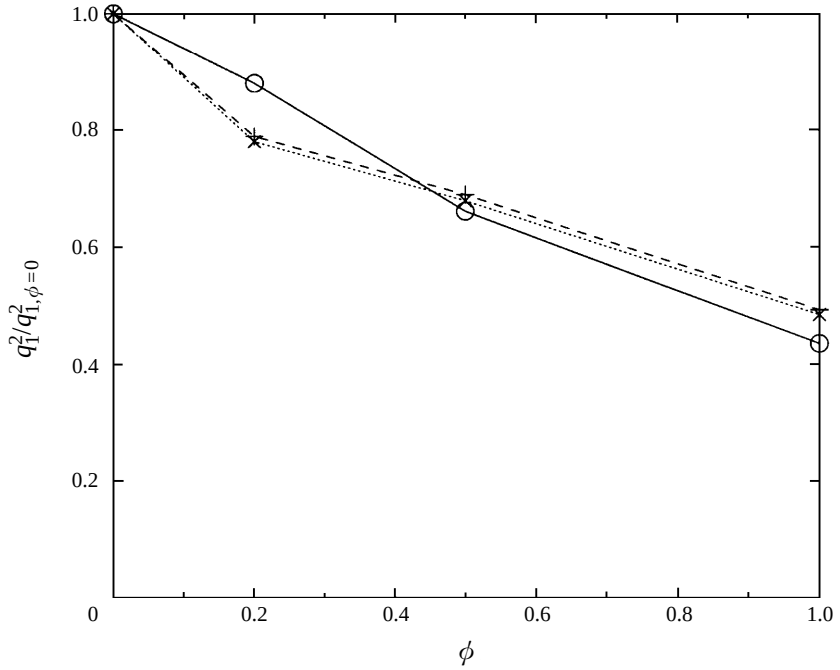

FIGURE 3. Turbulence kinetic energy q_1^2. O–O, $\tau_{12}^F = 0.064$; ×- - - -×, $\tau_{12}^F = 0.23$; + – – +, $\tau_{12}^F = 0.58$.

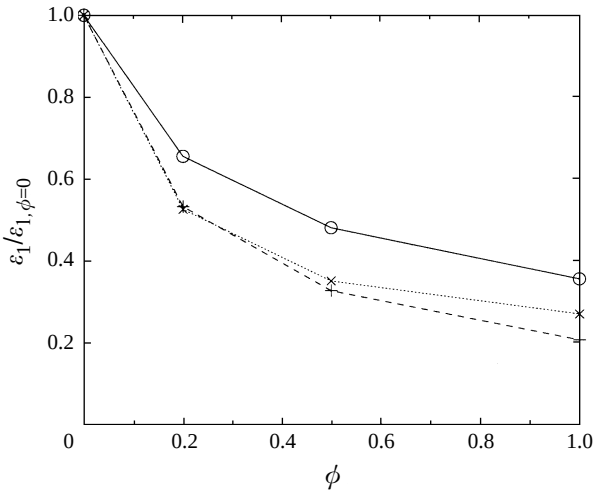

FIGURE 4. Dissipation rate ε_1. O–O, $\tau_{12}^F = 0.064$; ×- - - -×, $\tau_{12}^F = 0.23$; + – – +, $\tau_{12}^F = 0.58$.

time, which would have lead to a strong damping of high-wavenumber modes for particles with τ_{12}^F slightly greater than τ_k.

It is also interesting to consider the possibility of 'backscatter' of energy from small to large scales as a response of the flow to the relative increase in turbulence energy at small scales. In the context of this discussion, 'backscatter' is simply regarded as an inverse cascade of fluid energy at a given wavenumber. Shown in figure 6 is the evolution with respect to ϕ of the fluid transfer spectrum $T_{11,1}(k)$ (typically denoted in single-phase turbulence as $T(k)$) for the smallest particles that provide the largest

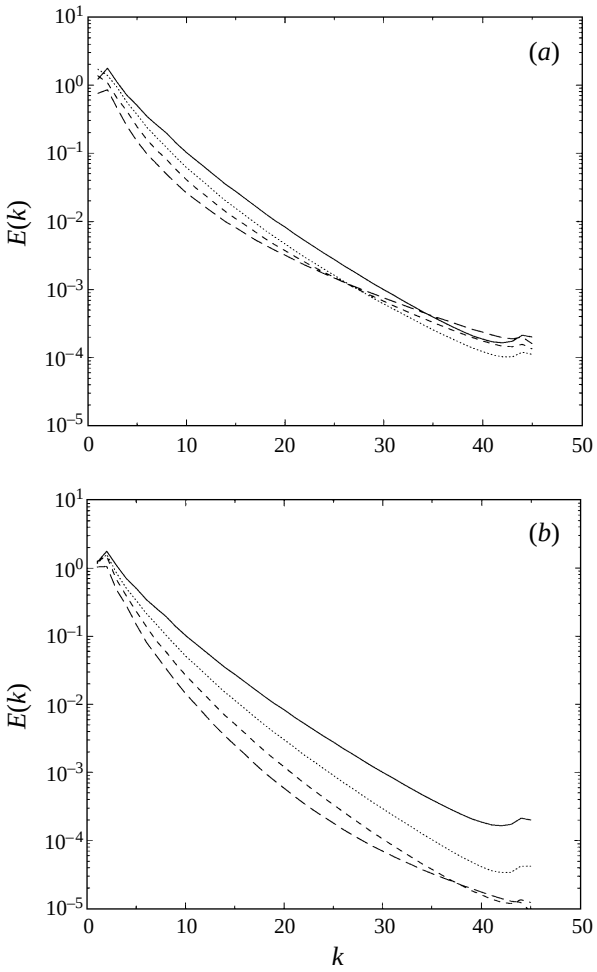

FIGURE 5. Turbulence kinetic energy spectrum. ———, $\phi = 0$; ·····, $\phi = 0.2$; – – – –, $\phi = 0.5$; — — —, $\phi = 1.0$. (*a*) $\tau_{12}^F = 0.064$; (*b*) $\tau_{12}^F = 0.58$.

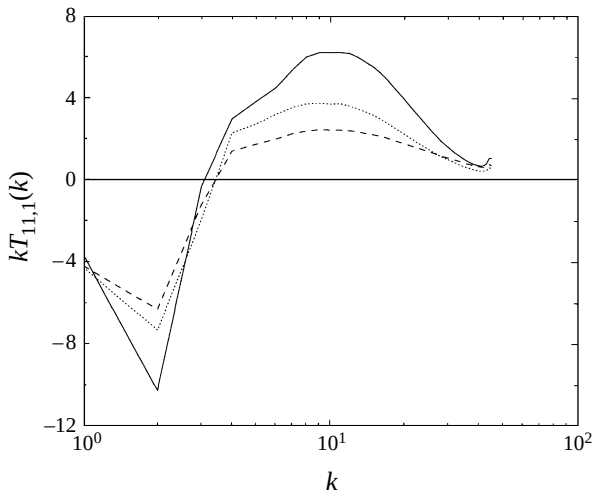

FIGURE 6. Turbulence transfer spectrum $T_{11,1}(k)$. ———, $\phi = 0$; $\tau_{12}^F = 0.064$: ·····, $\phi = 0.2$; – – – –, $\phi = 0.5$.

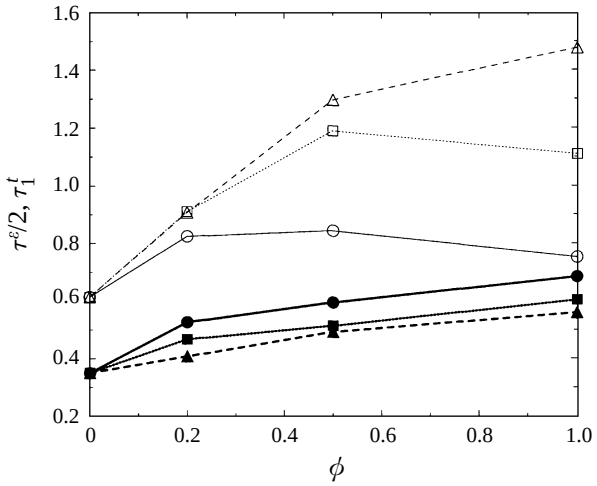

FIGURE 7. Time scales. Open symbols for the Eulerian time macro-scale $\tau^{\varepsilon}/2$; filled symbols for the fluid Lagrangian integral time scale τ_1^t. o–o, $\tau_{12}^F = 0.064$; □- - -□, $\tau_{12}^F = 0.23$; △– –△, $\tau_{12}^F = 0.58$.

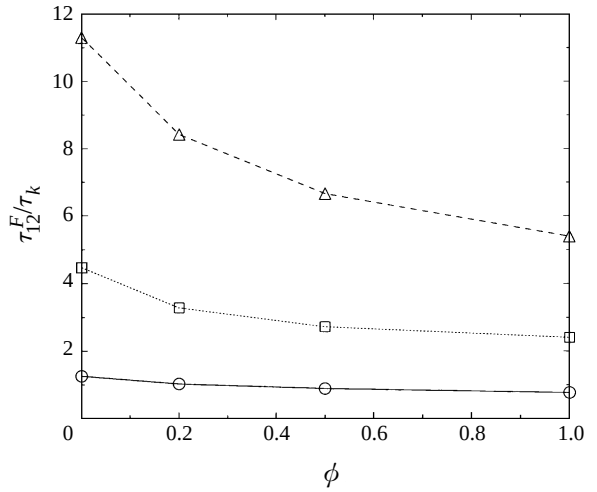

FIGURE 8. Ratio of the particle relaxation time τ_{12}^F to the Kolmogorov time scale τ_k. o–o, $\tau_{12}^F = 0.064$; □- - -□, $\tau_{12}^F = 0.23$; △– –△, $\tau_{12}^F = 0.58$.

enhancement of small-scale turbulent motions. The figure shows that, regardless of the value of ϕ, $T_{11,1}(k)$ has a form similar to that in single-phase flow with a transfer of energy from large to small scales. The result in figure 6 is similar to that obtained in decaying isotropic turbulence by Elghobashi & Truesdell (1993). Finally, it should be pointed out that to completely understand how two-way coupling affects nonlinear energy transfer in the fluid, a detailed study of triadic interactions is necessary (e.g. see Domaradzki, Liu & Brachet 1993).

The dependence of the Eulerian time macro-scale τ^{ε} and Lagrangian integral time scale τ_1^t on mass loading is shown in figure 7 and offers further insight into the effect of two-way coupling on the different behaviour exhibited by q_1^2 and ε_1. The Eulerian time macro-scale increases with larger mass loading, eventually reaching a maximum that occurs at larger ϕ for increasing τ_{12}^F. As is clear from the figure, the Lagrangian integral time scale exhibits a general increase with ϕ. Thus, assuming a

direct proportionality between these scales, as is often done in turbulence models, is not accurate for large mass loadings.

Shown in figure 8 is the ratio of the particle relaxation time to the Kolmogorov time scale. The figure shows that the ratio decreases with increasing mass loading, a consequence of the reduction in ε_1. This is in turn consistent with the effect of the larger particles on the flow being similar to that of the smaller particles as ϕ increases. For example, for $\tau_{12}^F = 0.58$ the spectrum $E(k)$ shows a relative increase of small-scale energy at high wavenumbers for $\phi = 1$, similar to that observed at smaller loadings for $\tau_{12}^F = 0.064$ (a similar feature may be observed in the spectrum of the fluid–particle energy exchange rate shown in figure 14). The reduction in the time scale ratios with increasing ϕ complicates interpretation of whether two-way coupling can be more accurately described using the ratio of the relaxation time to the time scale of the large eddies, τ_{12}^F/τ_e, or the time scale of the smallest eddies, τ_{12}^F/τ_k. To resolve this issue requires simulations at substantially higher Reynolds numbers than can be achieved using DNS in order to provide a much larger separation between τ_e and τ_k.

3.1.2. *Turbulence transport equations*

For statistically stationary isotropic turbulence modified by momentum exchange with particles, the transport equations for the fluid turbulence kinetic energy and dissipation rate are

$$-\varepsilon_1 + \Pi_{q_1} + F_{q_1} = 0, \tag{3.1}$$

$$\varepsilon_{d1} - \varepsilon_{d2} + \Pi_{\varepsilon_1} + F_{\varepsilon_1} = 0, \tag{3.2}$$

where ε_{d1} and ε_{d2} in (3.2) are the production by turbulent vortex stretching and viscous destruction of dissipation, respectively; ε_{d2} can be expressed in terms of $E(k)$ as

$$\varepsilon_{d2} = 4\nu_1^2 \int_0^\infty k^4 E(k)\mathrm{d}k. \tag{3.3}$$

As discussed, for example, in Smith & Reynolds (1991), production by turbulent vortex stretching, ε_{d1}, is characteristic of a spectral transfer in that it measures the stretching of all turbulent structures. The terms F_{q_1} and F_{ε_1} are the contributions from the forcing, Π_{q_1} is the fluid–particle energy exchange rate, and Π_{ε_1} the fluid–particle dissipation exchange rate:

$$\Pi_{q_1} = -\frac{\phi}{\tau_{12}^F}\left[2\langle q_1^2\rangle_2 - q_{12}\right], \quad \Pi_{\varepsilon_1} = -2\nu_1\frac{\phi}{\tau_{12}^F}\left\langle \frac{\partial u''_{1,i}}{\partial x_j}\frac{\partial (u''_{1,i} - u''_{2,i})}{\partial x_j}\right\rangle_2. \tag{3.4}$$

In (3.4), q_{12} is the fluid–particle velocity covariance, $\langle q_1^2\rangle_2$ is the fluid kinetic energy along the particle trajectory, $u''_{1,i}$ and $u''_{2,i}$ are the fluid and particle velocity fluctuations measured along the particle trajectory, respectively. Note that $\langle\cdot\rangle_2$ denotes averages over the dispersed phase.

The production of dissipation ε_{d1} by vortex stretching is shown in figure 9. The figure shows a large reduction with increasing ϕ and a weak dependence (reduction) on τ_{12}^F. The dependence on particle relaxation time appears stronger with increasing ϕ. Overall, ε_{d1} exhibits similar behaviour to that observed previously with ε_1 (cf. figure 4). The viscous destruction of dissipation ε_{d2} exhibits an interesting behaviour plotted in figure 10. It initially decreases with increases in loading. For the smallest particles, ε_{d2} attains a minimum for $\phi > 0.2$, which seems to preclude an increase at higher ϕ. The plateau in ε_{d2} occurs at higher ϕ with increasing τ_{12}^F. Note also that the

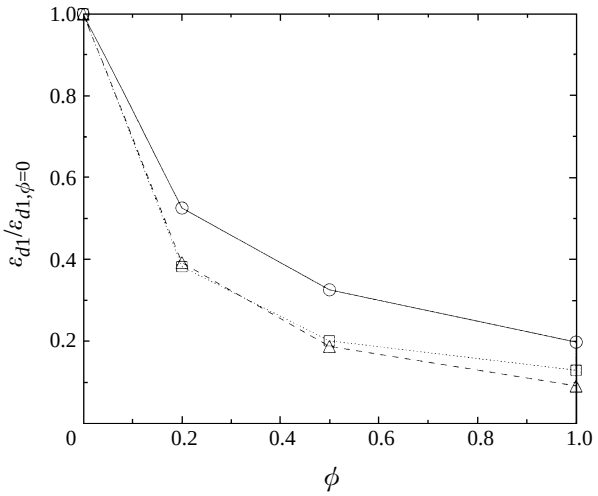

FIGURE 9. Production of dissipation ε_{d1}. O–O, $\tau_{12}^F = 0.064$; □- - -□, $\tau_{12}^F = 0.23$; △– –△, $\tau_{12}^F = 0.58$.

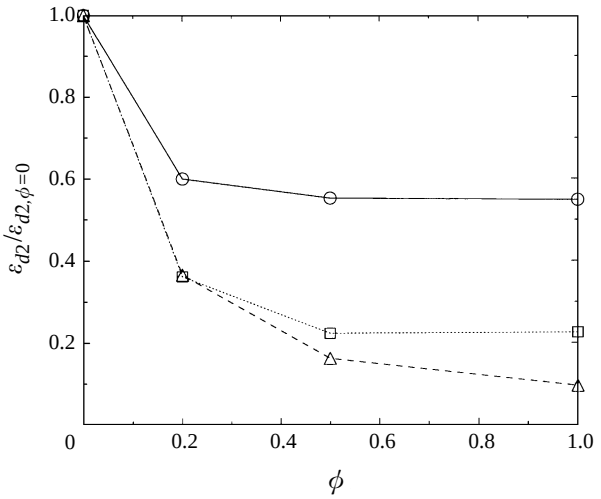

FIGURE 10. Viscous destruction of dissipation ε_{d2}. O–O, $\tau_{12}^F = 0.064$; □- - -□, $\tau_{12}^F = 0.23$; △– –△, $\tau_{12}^F = 0.58$.

plateau in ε_{d2} occurs at the same mass loadings as that observed at high wavenumbers in the energy spectra in figure 5.

Shown in figure 11 is the relative behaviour of ε_{d1} and ε_{d2}, the dissipation of the energy dissipation rate $\varepsilon_{\varepsilon_1} = \varepsilon_{d1} - \varepsilon_{d2}$, normalized by the quantity it is usually modelled by, $-\varepsilon_1^2/q_1^2$. In single-phase flows a balance exists between ε_{d1} and ε_{d2} and therefore these terms are modelled together (e.g. see Smith & Reynolds 1991). The ratio shown in figure 11 increases with ϕ except at low loadings for large particles where it actually becomes negative, indicating that the effect of the particles is to provide a source of dissipation. The results in the figure clearly show that modulation of the flow by particles can strongly disrupt the equilibrium between ε_{d1} and ε_{d2}. This in turn implies that $\varepsilon_{\varepsilon_1}$ must be modelled differently than in single-phase turbulence, with an explicit dependence on ϕ and τ_{12}^F (see Squires & Eaton 1994 for further discussion).

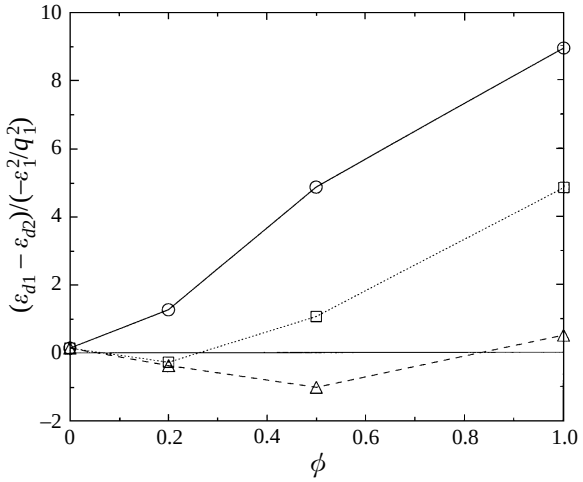

FIGURE 11. Dissipation of the energy dissipation rate, $(\varepsilon_{d1}-\varepsilon_{d2})/(-\varepsilon_1^2/q_1^2)$. O–O, $\tau_{12}^F = 0.064$; □- - -□, $\tau_{12}^F = 0.23$; △– –△, $\tau_{12}^F = 0.58$.

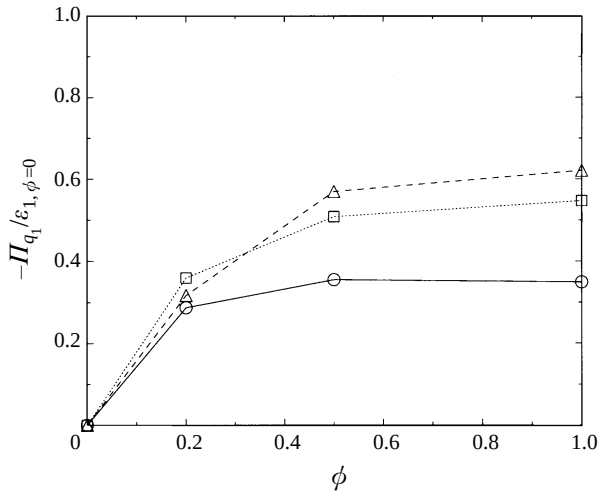

FIGURE 12. Particle dissipation normalized by fluid viscous dissipation $-\Pi_{q_1}/\varepsilon_{1,\phi=0}$. O–O, $\tau_{12}^F = 0.064$; □- - -□, $\tau_{12}^F = 0.23$; △– –△, $\tau_{12}^F = 0.58$.

3.2. *Particle source term statistics*

3.2.1. *Fluid–particle energy exchange rate*

On average, the particles are an additional dissipation of kinetic energy. The fluid–particle energy exchange rate Π_{q_1} is therefore negative. When normalized by $\varepsilon_{1,\phi=0}$, the evolution of $-\Pi_{q_1}$ displayed in figure 12 shows that dissipation by drag increases with particle size and mass loading. However, the figure also shows that $-\Pi_{q_1}/\varepsilon_{1,\phi=0}$ appears to reach a plateau for larger ϕ. The increasingly large contribution of the particles to the total dissipation with larger ϕ is shown more clearly in figure 13 where the ratio of the particle dissipation $-\Pi_{q_1}$ normalized by the total value is shown. It should be noted that production of kinetic energy by the forcing, F_{q_1}, exhibits a slight reduction with increased loading due to the fact that F_{q_1} measures

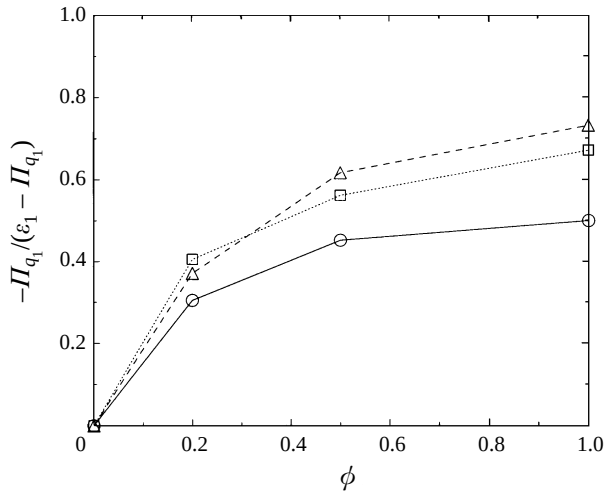

FIGURE 13. Particle dissipation normalized by total dissipation $-\Pi_{q_1}/(\varepsilon_1 - \Pi_{q_1})$. ○–○, $\tau_{12}^F = 0.064$; □- - -□, $\tau_{12}^F = 0.23$; △– –△, $\tau_{12}^F = 0.58$.

the correlation between the forcing acceleration and the low-wavenumber modes of the velocity which decrease for increasing ϕ.

The spectrum of the fluid–particle energy exchange rate, $\Pi_{q_1}(k)$, is shown in figure 14. The spectra display two regions: the low-wavenumber portion of the spectrum shows that the fluid turbulent motion transfers energy to the particles, i.e. the particles act as a sink of kinetic energy; at higher wavenumbers the spectrum of the energy exchange rate is positive, indicating that particles are capable of adding kinetic energy to the turbulence. This energy 'released' by the particles is not immediately dissipated by viscous effects but is in fact responsible for the relative increase of small-scale energy previously observed in the energy spectra (cf. figure 5*a*). Thus, the larger-scale motions occurring at lower wavenumbers drag the particles, while the converse is true for the smaller-scale motions at high wavenumbers.

As shown in figure 14, the drag of the fluid by the particles is more apparent at smaller relaxation times and for larger loadings, e.g. for $\tau_{12}^F = 0.58$, shown in figure 14(*b*), there is essentially no wavenumber range over which particles impart kinetic energy to the fluid. The figures also show that the absolute value of the negative portion of the spectrum increases weakly with τ_{12}^F, indicating that the magnitude of Π_{q_1} is an increasing function of τ_{12}^F. This is in accordance with the results for Π_{q_1} shown in figure 12. For increasing ϕ, the region of positive $\Pi_{q_1}(k)$ increases in magnitude and the corresponding wavenumber range also shifts towards larger scales.

3.2.2. *Fluid–particle dissipation exchange rate*

The source term representing the direct effect of the particles on the dissipation rate, Π_{ε_1}, is shown in figure 15. This quantity undergoes the most striking evolution of the turbulence quantities. For small ϕ it acts as a sink of dissipation, with the exception of the smallest particles, before becoming a source of dissipation as the loading increases. The loading ratio at which Π_{ε_1} changes from sink to source also increases with τ_{12}^F. The evolution of Π_{ε_1} can be more clearly understood from its definition:

$$\Pi_{\varepsilon_1} = \int_0^\infty \Pi_{\varepsilon_1}(k)\,\mathrm{d}k = \int_0^\infty 2\nu_1 k^2 \Pi_{q_1}(k)\,\mathrm{d}k. \tag{3.5}$$

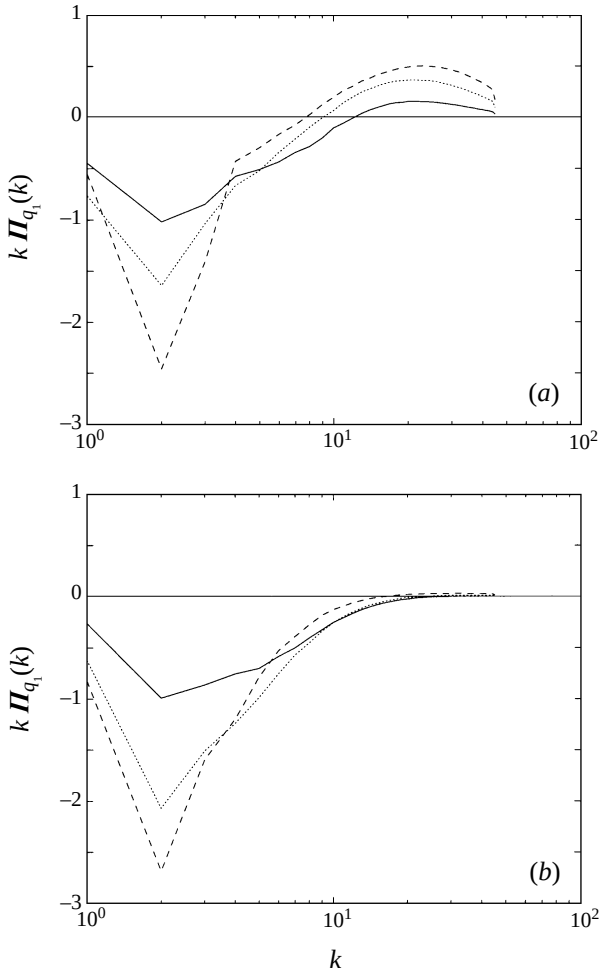

FIGURE 14. Spectrum of the fluid-particle energy exchange rate, $\Pi_{q1}(k)$. ———, $\phi = 0.2$; ·····, $\phi = 0.5$; – – – –, $\phi = 1.0$. (*a*) $\tau_{12}^F = 0.064$; (*b*) $\tau_{12}^F = 0.58$.

Particles with small relaxation times drag the fluid at small scales, an effect which increases with larger loading. The weighting of the high wavenumbers in (3.5) accentuates this effect, ultimately causing Π_{ε_1} to act as a source of dissipation.

3.3. *Spectral analysis*

The spectral equations for the fluid turbulence, particle fluctuating velocities, and fluid–particle covariance are obtained by manipulation of (2.7) and (2.10) (e.g. see Baw & Peskin 1971). These equations allow one to form the appropriate two-point correlations from which Fourier transformation can then be applied to obtain the transport equations in spectral space.

In homogeneous isotropic turbulence, a projector can be used to pass from directional to tridimensional quantities. Its application to the spectral equations followed by an integration over angular variables yields equations governing the fluid turbulence energy spectrum, $E_{11}(k)$, the energy spectrum of the fluid turbulence along the particle trajectory, $E_{11,2}(k)$, the fluid–particle covariance spectrum, $E_{12}(k)$, and the particle energy spectrum, $E_{22}(k)$. For wavenumbers k greater than K_F (the radius

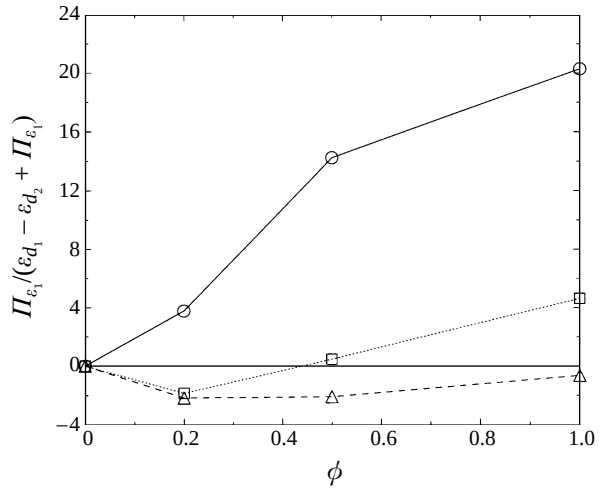

FIGURE 15. Fluid-particle dissipation exchange rate normalized by total dissipation rate $\Pi_{\varepsilon_1}/(\varepsilon_{d1} - \varepsilon_{d2} + \Pi_{\varepsilon_1})$. O–O, $\tau_{12}^F = 0.064$; □- - -□, $\tau_{12}^F = 0.23$; △– –△, $\tau_{12}^F = 0.58$.

of the spectral sphere of the forced modes) for which the forcing contribution is identically nul these equations are

$$\frac{\partial}{\partial t}E_{11}(k) = T_{11,1}(k) - 2\nu_1 k^2 E_{11}(k) + \Pi_{q_1}(k), \tag{3.6}$$

$$\frac{\partial}{\partial t}E_{12}(k) + \left[\frac{1+\phi}{\tau_{12}^F} + \nu_1 k^2\right] E_{12}(k) = T_{12,1}(k) + T_{12,2}(k) + \frac{2}{\tau_{12}^F}\left[E_{11,2}(k) + \phi E_{22}(k)\right], \tag{3.7}$$

$$\frac{\partial}{\partial t}E_{22}(k) = T_{22,2}(k) - \frac{1}{\tau_{12}^F}\left[2E_{22}(k) - E_{12}(k)\right], \tag{3.8}$$

$$\Pi_{q_1}(k) = -\frac{\phi}{\tau_{12}^F}\left[u'_{1,i}(k)(u_{1,i} - u_{2,i})(k)\right] \tag{3.9}$$

(see Baw & Peskin 1971; Boivin 1996). The integrals corresponding to the spectra are

$$\left.\begin{aligned} q_1^2 &= \int_0^\infty E_{11}(k)\,\mathrm{d}k, \qquad \langle q_1^2\rangle_2 = \int_0^\infty E_{11,2}(k)\,\mathrm{d}k, \\ q_2^2 &= \int_0^\infty E_{22}(k)\,\mathrm{d}k, \qquad q_{12} = \int_0^\infty E_{12}(k)\,\mathrm{d}k. \end{aligned}\right\} \tag{3.10}$$

The terms $T_{11,1}$, $T_{12,1}$, $T_{12,2}$ and $T_{22,2}$ represent nonlinear energy transfer in the fluid turbulence, transfers of the fluid–particle correlated motion by the fluid turbulence along the particle–path, and by the particle fluctuating motion, and the transfer of particle-particle correlated motion by the particle motion, respectively. It should be noted that $\Pi_{q_1}(k)$ was computed according to its formal definition given above in (3.9). For non-settling particles in homogeneous isotropic turbulence, $\Pi_{q_1}(k)$ can also be expressed in terms of $E_{11,2}$ and E_{12} as

$$\Pi_{q_1}(k) = -\frac{\phi}{\tau_{12}^F}\left[E_{11,2}(k) - E_{12}(k)\right]. \tag{3.11}$$

The integral of (3.11) gives (3.4). In the solution of the equations developed below, $E_{11,2}(k)$ is approximated by $E_{11}(k)$, corresponding to an assumption of negligible differences in turbulence properties measured along particle trajectories compared

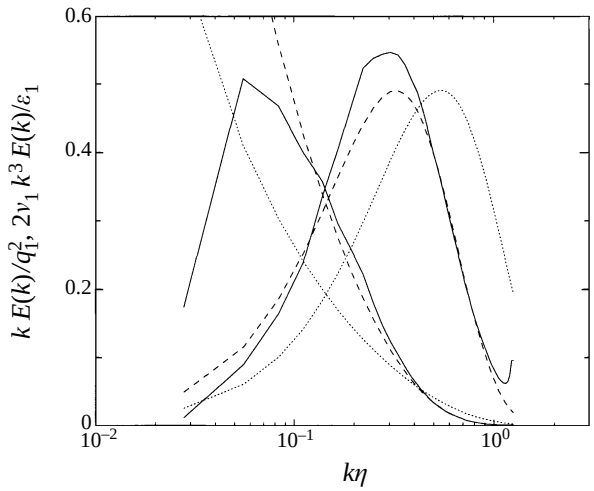

FIGURE 16. Normalized turbulence energy and dissipation spectra, $\phi = 0$. DNS: ——— ; Pao's spectra: ·····, $\alpha = 1.5$; – – – –, $\alpha = 3$.

with those on the grid. For a statistically stationary flow such as that considered in this work, the time derivatives are zero. Closure of the system (3.6)–(3.9) then requires models for the transfer terms.

3.3.1. *Closure of the transfer terms – unloaded flows*

For monophase turbulent flow, Pao (1965) proposed a form for $T_{11,1}(k)$ valid in the universal equilibrium range that respects the $-5/3$ slope in the inertial sub-range with a stronger damping of energy in the dissipative range. Pao (1965) assumed that the energy flux $S(k)$ through wavenumber k is directly proportional to $E(k)$, the energy density at wavenumber k. From a dimensional analysis, $S(k)$ can be expressed as

$$S(k) = \alpha^{-1}\varepsilon_1^{1/3}k^{5/3}E(k) \quad \text{with} \quad T(k) = -\frac{\mathrm{d}S(k)}{\mathrm{d}k}, \tag{3.12}$$

where α is the Kolmogorov constant. For zero mass loading the fluid turbulence spectral equation becomes for high Reynolds number turbulence

$$\frac{\mathrm{d}}{\mathrm{d}k}\alpha^{-1}\varepsilon_1^{1/3}k^{5/3}E(k) = -2\nu_1 k^2 E(k), \tag{3.13}$$

whose solution is

$$E(k) = \alpha\varepsilon_1^{2/3}k^{-5/3}\exp(-3/2\alpha(k\eta)^{4/3}). \tag{3.14}$$

Figure 16 compares the theoretical energy and dissipation spectra with those from the simulations at zero mass loading. The theoretical result can reproduce quite correctly the simulation results provided that $\alpha = 3$, rather than the usual value of 1.5 valid for high Reynolds number turbulence.

3.3.2. *Closure of the transfer terms – loaded flows*

In two-phase flows with two-way coupling, Baw & Peskin (1971) assumed that $T_{11,1}(k)$ can be expressed similarly as in single-phase turbulence in which viscous dissipation is equal to the energy transfer rate from the large scales. In an equilibrium forced turbulence the rate of energy transfer from the large scales, via the forcing, is dissipated by viscous effects in the fluid or by drag around the particles, i.e.

$F_{q_1} = \varepsilon_1 - \Pi_{q_1}$. Thus, the energy transfer rate appropriate for a spectral analysis of two-way coupling is the total dissipation, $\varepsilon_1 - \Pi_{q_1}$, rather than simply ε_1 as in single-phase turbulence. Therefore, we propose to replace ε_1 by the energy transfer rate for two-way coupling, $\varepsilon_1 - \Pi_{q_1}$, in the expression for $S(k)$. The transfer term $T_{11,1}(k)$ can then be written as

$$T_{11,1}(k) = -\frac{\mathrm{d}}{\mathrm{d}k}\alpha^{-1}(\varepsilon_1 - \Pi_{q_1})^{1/3}k^{5/3}E_{11}(k). \tag{3.15}$$

For $T_{12,1}(k)$, a closure analogous to that used in single-phase turbulence is adopted. The terms $T_{11,1}(k)$ and $T_{12,1}(k)$ are similar in that $T_{11,1}$ represents the transfer of fluid–fluid correlated motion by the fluid turbulence and $T_{12,1}$ represents the transfer of fluid–particle correlated motion by the fluid. Therefore, it is appropriate to replace E_{11} in (3.15) by E_{12}, while maintaining the same rate of energy transfer $\varepsilon_1 - \Pi_{q_1}$, i.e.

$$T_{12,1}(k) = -\frac{\mathrm{d}}{\mathrm{d}k}\alpha^{-1}(\varepsilon_1 - \Pi_{q_1})^{1/3}k^{5/3}E_{12}(k). \tag{3.16}$$

Baw & Peskin (1971) assumed that, due to particle inertia, $T_{12,1}$, $T_{12,2}$ and $T_{22,2}$ should be very small and can be neglected. It seems rather hazardous to imagine particle fluctuating motion similar to the fluid turbulence with a cascade of energy, etc. Thus, the development of closure models for $T_{12,2}$ and $T_{22,2}$, representing nonlinear energy transfer by the particle fluctuating motion, would require a completely different approach than that typically proposed for $T_{11,1}$. Spectral closures for $T_{12,2}$ and $T_{22,2}$ are not within the scope of this work and are therefore neglected.

With the approximations described above, the system of spectral equations becomes

$$\frac{\mathrm{d}\left[\alpha^{-1}(\varepsilon_1 - \Pi_{q_1})^{1/3}k^{5/3}E_{11}(k)\right]}{\mathrm{d}k} = -2\nu_1 k^2 E_{11}(k) - \frac{\phi}{\tau_{12}^F}\left[2E_{11}(k) - E_{12}(k)\right], \tag{3.17}$$

$$\frac{\mathrm{d}\left[\alpha^{-1}(\varepsilon_1 - \Pi_{q_1})^{1/3}k^{5/3}E_{12}(k)\right]}{\mathrm{d}k} = -\left[\frac{1}{\tau_{12}^F} + \nu_1 k^2\right]E_{12}(k) + \frac{2}{\tau_{12}^F}E_{11}(k), \tag{3.18}$$

$$E_{22}(k) = \tfrac{1}{2}E_{12}(k). \tag{3.19}$$

3.3.3. *Model without* $T_{12,1}$

If one neglects the transfer of the fluid–particle covariance by the fluid turbulence, $T_{12,1}$, then the only differential equation to solve is that for E_{11}. The system (3.17)–(3.19) in this case is identical to that obtained by Baw & Peskin (1971) with $\varepsilon_1 - \Pi_{q_1}$ instead of ε_1 as the rate of transfer,

$$\frac{\mathrm{d}\left[\alpha^{-1}(\varepsilon_1 - \Pi_{q_1})^{1/3}k^{5/3}E_{11}(k)\right]}{\mathrm{d}k} = -2\nu_1 k^2 E_{11}(k) - \frac{\phi}{\tau_{12}^F}\left[2E_{11}(k) - E_{12}(k)\right], \tag{3.20}$$

$$E_{12}(k) = \frac{2}{1 + \nu_1 k^2 \tau_{12}^F}E_{11}(k), \tag{3.21}$$

$$E_{22}(k) = \tfrac{1}{2}E_{12}(k). \tag{3.22}$$

Using (3.21), the term due to the modulation of the turbulence by particles in the expression (3.20) for E_{11} can be expressed as

$$-\frac{\phi}{\tau_{12}^F}\left[2E_{11}(k) - E_{12}(k)\right] = -2\phi\frac{\nu_1 k^2}{1 + \nu_1 k^2 \tau_{12}^F}E_{11}(k). \tag{3.23}$$

The right-hand side of (3.23) is negative definite, indicating that particles act as a sink in (3.20) across the spectrum. This is in contrast, however, to the results presented in §3 which showed that there can be an increase in the high-wavenumber components of the fluid turbulence, e.g. for the smaller particles at higher mass loadings.

3.3.4. *Model with* $T_{12,1}$

Inclusion of the closure model for $T_{12,1}$ requires solution of (3.18). It is also important to point out that the term accounting for the modulation of the fluid spectrum, $\Pi_{q_1}(k)$, is changed by the inclusion of $T_{12,1}$. Solving (3.7) for E_{12} and substitution into (3.11) yields

$$\Pi_{q_1}(k) = -\frac{\phi}{\tau_{12}^F}\left[2E_{11}(k) - E_{12}(k)\right]$$

$$= -2\phi\frac{v_1 k^2}{1 + v_1 k^2 \tau_{12}^F} E_{11}(k) + \frac{\phi}{1 + v_1 k^2 \tau_{12}^F} T_{12,1}(k). \tag{3.24}$$

The contribution in $\Pi_{q_1}(k)$ from $T_{12,1}(k)$ should be positive at high wavenumbers and can therefore balance the negative contribution from $E_{11}(k)$. This is in turn consistent with the change of sign in $\Pi_{q_1}(k)$ observed in figure 14. Note also that the factor in front of $T_{12,1}$ increases with ϕ and decreases with τ_{12}^F. Moreover, the motion of larger particles is less correlated with the fluid, which should in turn reduce the fluid–particle covariance transfer (cf. (3.16)). Thus, inclusion of the transfer term $T_{12,1}$ appears to behave in accordance with the evolution of the small-scale motions observed in the DNS.

3.3.5. *Numerical resolution*

The solution of (3.20)–(3.22) is more easily accomplished by defining new variables:

$$G_{11}(k) = 1/\beta_1\, k^{5/3}\, E_{11}(k), \quad \beta_1 = \alpha(\varepsilon_1 - \Pi_{q_1})^{-1/3}, \tag{3.25}$$

$$G_{12}(k) = 1/\beta_2\, k^{5/3}\, E_{12}(k), \quad \beta_2 = \alpha(\varepsilon_1 - \Pi_{q_1})^{-1/3}. \tag{3.26}$$

The general system (3.17)–(3.19) becomes for all k greater than K_F

$$\frac{\mathrm{d}G_{11}(k)}{\mathrm{d}k} = \beta_1\left[-2v_1 k^{1/3} - 2\frac{\phi}{\tau_{12}^F}k^{-5/3}\right] G_{11}(k) + \beta_1\frac{\phi}{\tau_{12}^F}k^{-5/3}\, G_{12}(k), \tag{3.27}$$

$$\frac{\mathrm{d}G_{12}(k)}{\mathrm{d}k} = \beta_2\frac{2}{\tau_{12}^F}k^{-5/3}\, G_{11}(k) + \beta_2\left[-v_1 k^{1/3} - \frac{1}{\tau_{12}^F}k^{-5/3}\right] G_{12}(k). \tag{3.28}$$

The system (3.27)–(3.28) can be solved numerically for both non-zero and zero values of $\mathrm{d}G_{12}(k)/\mathrm{d}k$, corresponding to inclusion or neglect of $T_{12,1}$ in the spectral equations. Because $E_{11}(k)$ and presumably $E_{12}(k)$ decrease more rapidly than $k^{-5/3}$, conditions on $G_{11}(k)$ and $G_{12}(k)$ are $G_{11}(\infty) = G_{12}(\infty) = 0$. However, these conditions are not convenient for numerical solution. In order to facilitate comparison between the DNS results and theoretical predictions, the spectral values at $k = 4$ were used to solve (3.27)–(3.28). Note from figure 16 that $k = 4$ corresponds to the beginning of the region in which there is good agreement between the DNS results and theory for zero mass loading.

Figure 17 compares the predicted spectra, with and without the closure (3.16) for $T_{12,1}$, to the DNS results for $\tau_{12}^F = 0.064$ and $\tau_{12}^F = 0.58$, both at $\phi = 1$. For $\tau_{12}^F = 0.064$, inclusion of $T_{12,1}$ is crucial to obtaining a very good agreement between the DNS results and model prediction. In particular, the model prediction does not roll off as

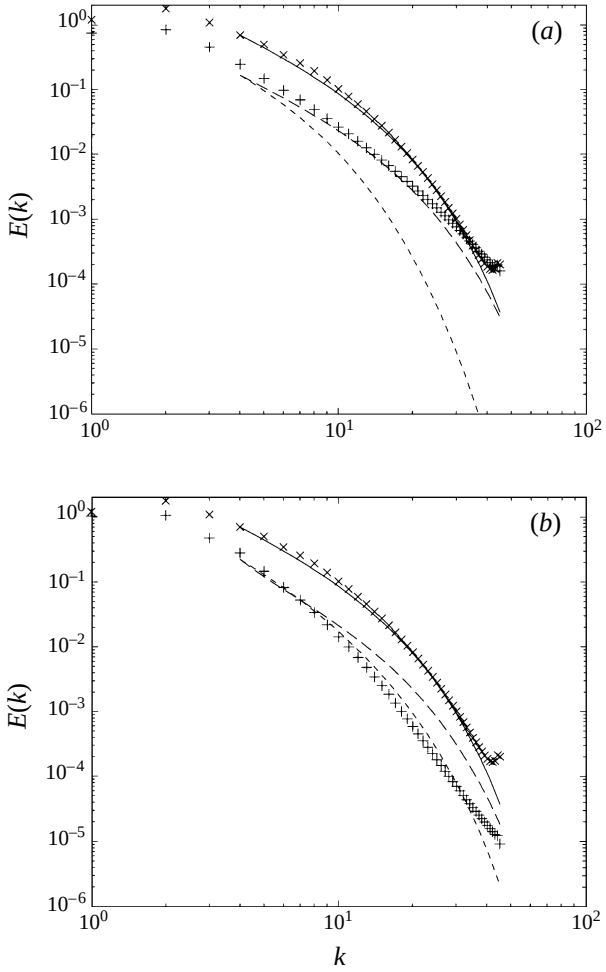

FIGURE 17. Normalized turbulence energy spectrum. DNS: ×, $\phi = 0$; +, $\phi = 1$. Predicted: ———, $\phi = 0$; $\phi = 1$: – – – –, model without $T_{12,1}$; — — —, model with $T_{12,1}$. (*a*) $\tau_{12}^F = 0.064$; (*b*) $\tau_{12}^F = 0.58$.

rapidly at high wavenumbers and also respects the relative increase of small-scale energy observed in the DNS. For $\tau_{12}^F = 0.58$, the system (3.20)–(3.22) (neglecting $T_{12,1}$) is in reasonable agreement with the DNS results and figure 17 shows that inclusion of the model for $T_{12,1}$ tends to over estimate $E(k)$. As shown in the figure, however, the smaller contribution for $\tau_{12}^F = 0.58$ does not sufficiently damp $T_{12,1}$ for the larger particles. This implies that a more accurate model for the transfer of the fluid–particle covariance should have an explicit dependence on τ_{12}^F.

Figures 18(*a*) and 18(*b*) demonstrate the effect of $T_{12,1}$ on the fluid–particle energy exchange. Shown in the figure is the modelled and actual form of the spectrum of the fluid–particle energy exchange rate, $\Pi_{q_1}(k)$. The contributions of the terms in (3.24) are also shown. The figure shows that at least qualitatively the prediction (3.24), including the transfer $T_{12,1}$, can reproduce the overall behaviour in $\Pi_{q_1}(k)$. In particular, the contribution of the transfer of fluid–particle covariance by fluid turbulence succeeds in making $\Pi_{q_1}(k)$ positive at high wavenumbers for the small particles. The integral value of the positive portion of $\Pi_{q_1}(k)$ is indeed inversely proportional to τ_{12}^F and the

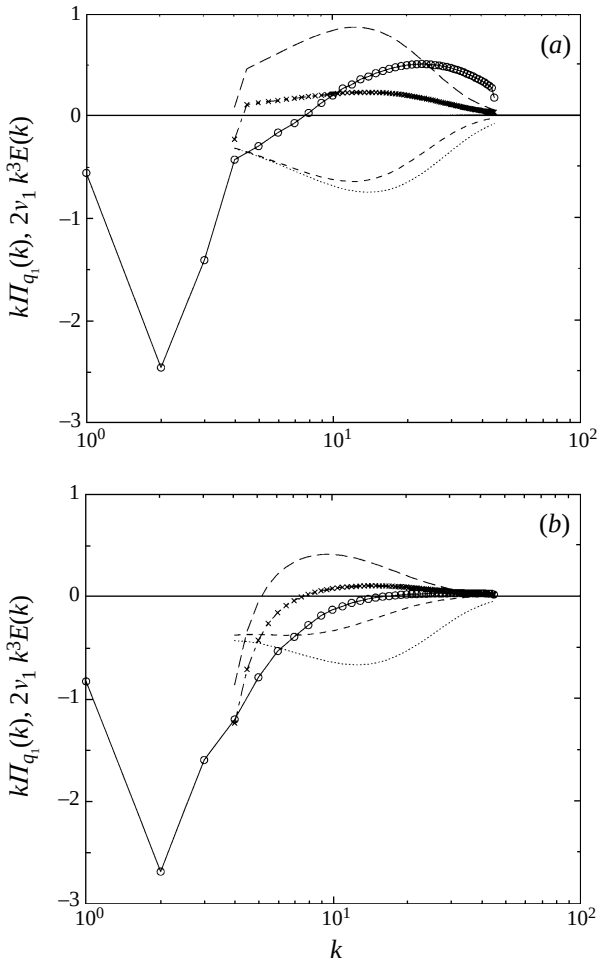

FIGURE 18. Spectrum of the fluid-particle energy exchange rate, $\Pi_{q_1}(k)$, $\phi = 1$. ○–○, DNS; equation (3.24): – – – –, $E_{11}(k)$ contribution; — — —, $T_{12,1}$ contribution; ×— – —×, equation (3.24). ·····, dissipation spectrum obtained from (3.24). (*a*) $\tau_{12}^F = 0.064$; (*b*) $\tau_{12}^F = 0.58$.

wavenumber at which the effect of the particles changes from a sink to a source of turbulence energy also increases with τ_{12}^F, in agreement with DNS results.

Figure 18 also shows that $\Pi_{q_1}(k)$ is overestimated at the lower wavenumbers. One factor influencing the overestimation is the neglect of $T_{12,2}$ in the transport equation for E_{12}. If it is assumed that $T_{12,2}$ is analogous to nonlinear transfers in the fluid, $T_{11,1}$ and $T_{12,1}$, then $T_{12,2}$ would be composed of two portions, negative at low wavenumbers and positive at higher wavenumbers. In the spectral equation (3.7) for $E_{12}(k)$, $T_{12,2}$ would then be a sink at low wavenumbers and a source at high wavenumbers. At the large scales this would result in a reduction in $E_{12}(k)$ and, according to (3.11), a decrease of $\Pi_{q_1}(k)$ at low wavenumbers. Similarly, the relative increase in $\Pi_{q_1}(k)$ at high wavenumbers due to the contribution from $T_{12,2}$ would also reduce the discrepancy between model predictions and DNS results in figure 18.

4. Summary and conclusions

Direct numerical simulation of the incompressible Navier–Stokes equations has been used to investigate turbulence modulation by particles in isotropic turbulence. The flow field was forced at the low wavenumbers to maintain a statistically stationary condition. Three relaxation times ranging from the Kolmogorov time scale to the Eulerian time scale of the reference fluid flow ($\phi = 0$) and loading ratios ϕ ranging from 0 to 1 comprised the particle parameter space.

For non-zero mass loading, particles increasingly dissipate fluid kinetic energy as the loading ratio increases, with the reduction in the kinetic energy being relatively independent of the relaxation time. Simultaneously, viscous dissipation in the fluid decreases with increases in ϕ, being larger for particles with smaller relaxation times. Furthermore, the ratio of the kinetic energy to the dissipation rate, that defines the Eulerian time macro-scale τ^{ε}, differs noticeably from that of the fluid Lagrangian integral time scale τ_1^t, which increases with ϕ. The different response of quantities such as the kinetic energy and dissipation rate to increased loading and changes in particle relaxation time is in turn linked to the fluid turbulence energy spectra. DNS results show that there is a non-uniform distortion of $E(k)$, with a relative increase in small-scale energy. The non-uniform distortion significantly affects the transport of ε_1 since the production of dissipation ε_{d1} and destruction of dissipation ε_{d2} exhibit completely different behaviours. For example, for small relaxation times and large mass loadings, particles can be a source of dissipation, rather than a sink as conventionally modelled.

The fluid–particle energy exchange rate, Π_{q_1}, increases relative to the total dissipation for both larger loading and relaxation time. The spectrum $\Pi_{q_1}(k)$ shows that, while the larger eddies drag the particles, particles with small τ_{12}^F drag the fluid increasingly at larger loading. Thus, particles 'release' to turbulent small-scale motions part of the energy extracted from the larger scales. This phenomenon in turn explains the switch from sink to source of the fluid–particle dissipation exchange rate Π_{ε_1} that occurs at lower ϕ for small particles.

A spectral analysis shows that the increase of the high-wavenumber portion of the fluid energy spectrum can be attributed to transfer of the fluid–particle covariance by the fluid turbulence. A closure analogous to that employed in single-phase turbulence was used to model transfer of the fluid–particle covariance and incorporation of this closure improves predictions of the fluid energy spectrum more for cases in which smaller particles modify the turbulence, as compared with modification by larger particles (cf. figure 17). This closure was developed independently of any structural interactions occurring between particles and turbulence, such as those arising from preferential concentration which would be more significant for the smallest particles (at least at low loadings). While preferential concentration is an important phenomena, the more accurate model prediction of the fluid energy spectrum obtained for the smaller particles would indicate an explicit accounting of this effect was not crucial for predicting the overall spectral evolution of the fluid turbulence.

While the approach used in the present study – DNS – is appropriate for detailed analyses of particle-turbulence interactions, there are issues relevant to two-way coupling which cannot be resolved using direct simulations. The low Reynolds numbers and limited range of scales in DNS, for example, prevent a determination of whether two-way coupling is best described in terms of large- or small-scale variables, i.e. in terms of τ_{12}^F/τ_e or τ_{12}^F/τ_k. Because of the 'global' distortion of the turbulence across the entire spectrum, a description of two-way coupling in terms of small-scale

variables may not be the most appropriate, as is conventionally assumed. Calculations at substantially higher Reynolds numbers are required in order to obtain a wide separation between the energy-containing and dissipating scales. While DNS of single-phase, isotropic turbulence can be performed at rather high Reynolds numbers, the computational constraints, e.g. adequate particle sample sizes, necessary for accurate resolution of two-way coupling may make exceedingly difficult the use of DNS to determine if the dominant processes in two-way coupling scale on large- or small-scale variables.

Financial support for this work is gratefully acknowledged from NASA (Grant NAG3-2081), the National Science Foundation (Grant OCE-94-09073), and the National Institute for Occupational Safety and Health (Grant Number OH03052-03). Computer time for some of the simulations was supplied by the Cornell Theory Center.

REFERENCES

Balachandar, S. & Maxey, M. R. 1989 Methods for evaluating fluid velocities in spectral simulations of turbulence. *J. Comput. Phys.* **83**, 96.

Baw, P. S. H. & Peskin, R. L. 1971 Some aspects of gas-solid suspension turbulence. *Trans. ASME* D: *J. Basic Engng*, 631.

Boivin, M. 1996 Etude de l'Influence des Particules sur la Turbulence a partir de Simulations Directes et de Simulations des Grandes Echelles d'ecoulements Diphasiques Gaz-Solides Homogenes Isotropes Stationnaires. PhD thesis, Université de Rouen.

Clift, R., Grace, J. R. & Weber, M. E. 1978 *Bubbles, Drops, and Particles*. Academic Press.

Comte-Bellot, G. & Corrsin, S. 1971 Simple Eulerian time correlation of full-and narrow-band velocity signals in grid-generated isotropic turbulence. *J. Fluid Mech.* **186**, 199.

Crowe, C. T. 1982 Review–numerical methods for dilute gas-particle flows. *Trans. ASME* I: *J. Fluids Engng* **104**, 297.

Crowe, C. T., Troutt, T. R. & Chung, J. N. 1996 Numerical models for two-phase turbulent flows. *Ann. Rev. Fluid Mech.* **28**, 11.

Csanady, G. T. 1963 Turbulent diffusion of heavy particles in the atmosphere. *J. Atmos. Sci.* **20**, 201.

Deutsch, E. & Simonin, O. 1991 Large eddy simulation applied to the modeling of particulate transport coefficients in turbulent two-phase flows. In *Proc. 8th Intl Symp. on Turbulent Shear Flows, Univ. of Munich*, vol. 1, p. 1011.

Domaradzki, J., Liu, W. & Brachet, M. 1993 An analysis of subgrid-scale interactions in numerically simulated isotropic turbulence. *Phys. Fluids* A **5**, 1747.

Elghobashi, S. E. & Truesdell, G. C. 1993 On the two-way interaction between homogeneous turbulence and dispersed solid particles. I: turbulence modification. *Phys. Fluids* A **5**, 1790.

Eswaran, V. & Pope, S. B. 1988 An examination of forcing in direct numerical simulations of turbulence. *Computers & Fluids*, **16**, 257.

Fleckhaus D., Hishida, K. & Maeda, M. 1987 Effect of laden solid particles on the turbulent flow structure of a round free jet. *Exps. Fluids*, **5**, 323.

Gatignol, R. 1983 The Faxén formulae for a rigid particle in an unsteady non-uniform Stokes flow. *J. Méc. Theor. Appl.* **1**, 143.

Gore, R. A. & Crowe, C. T. 1989 Effect of particle size on turbulence intensity. *Intl J. Multiphase Flow* **15**, 279.

Hardalupas, Y., Taylor, A. M. K. P. & Whitelaw, J. H. 1989 Velocity and particle-flux characteristics of turbulent particle-laden jets. *Proc. R. Soc. Lond.* A **426**, 31.

Hinze, JO. 1975 *Turbulence*. McGraw-Hill.

Koch, D. 1990 Kinetic theory for a monodisperse gas-solid suspension. *Phys. Fluids* A **2**, 1711–1723.

Kulick, J. D., Fessler, J. R. & Eaton J. K. 1994 Particle response and turbulence modification in fully developed channel flow. *J. Fluid Mech.* **277**, 109.

MAXEY, M. R., PATEL, B. K. & WANG, L.-P. 1997 Simulations of dispersed turbulent multiphase flow. *Fluid Dyn. Res.* **20** 143.

MAXEY, R. & RILEY, J. 1983 Equation of motion for a small rigid sphere in a turbulent fluid flow. *Phys. Fluids* **26**, 883.

MODARRESS, D., TAN, H. & ELGHOBASHI, S. E. 1984 Two component LDA measurement in a two-phase turbulent jet. *AIAA J.* **22**, 624.

PAO, Y. H. 1965 Structure of turbulent velocity and scalar fields at large wavenumbers. *Phys. Fluids* **8**, 1063.

ROGALLO, R. S. 1981 Numerical experiments in homogeneous turbulence. *NASA Tech. Mem.* 81835.

ROGERS, C. B. & EATON, J. K. 1991 The effect of small particles on fluid turbulence in a flat-plate turbulent boundary layer in air. *Phys. Fluids* A **3**, 928.

SAFFMAN, P. G. 1973 On the settling speed of free and fixed suspension. *Stud. Appl. Maths* **52**, 115–127.

SHUEN, J.-S., SOLOMON, A. S. P., ZHANG, Q.-F. & FAETH, G. M. 1985 Structure of particle-laden jets: measurements and predictions. *AIAA J.* **23**, 396.

SIMONIN, O., DEUTSCH, E. & BOIVIN, M. 1995 Large eddy simulation and second-moment closure model of particle fluctuating motion in two-phase turbulent shear flows. In *Selected Papers from the Ninth Intl Symp. on Turbulent Shear Flows* (ed. F. Durst, N. Kasagi, B. E. Launder, F. W. Schmidt, K. Suzuki & J. H. Whitelaw), p. 85. Springer.

SIMONIN, O., DEUTSCH, E. & MINIER, J. P. 1993 Eulerian prediction of the fluid/particle correlated motion in turbulent two-phase flows. *Appl. Sci. Res.* **5**, 275.

SMITH, L. M. & REYNOLDS, W. C. 1991 The dissipation-range spectrum and the velocity derivative skewness in turbulent flows. *Phys. Fluids* A **3**, 992.

SQUIRES, K. D. & EATON, J. K. 1990 Particle response and turbulence modification in isotropic turbulence. *Phys. Fluids* A **2**, 1191.

SQUIRES, K. D. & EATON, J. K. 1991*a* Preferential concentration of particles by turbulence. *Phys. Fluids* A **3**, 1169.

SQUIRES, K. D. & EATON, J. K. 1991*b* Measurements of particle dispersion obtained from direct numerical simulations of isotropic turbulence. *J. Fluid Mech.* **226**, 1.

SQUIRES, K. D. & EATON, J. K. 1994 Effect of selective modification of turbulence on two-equation models for particle-laden turbulent flows. *Trans. ASME* I: *J. Fluids Engng* **116**, 778.

SUNDARAM, S. & COLLINS, L. R. 1996 Numerical considerations in simulating a turbulent suspension of finite-volume particles. *J. Comput. Phys.* **124**, 337.

TSUJI, Y., MORIKAWA, Y. & SHIOMI, H. 1984 LDV measurements of an air-solid two-phase flow in a vertical pipe. *J. Fluid Mech.* **139**, 417.

UNVERDI, S. O. & TRYGGVASON, G. 1992 A front-tracking method for viscous, incompressible, multi-fluid flows. *J. Comput. Phys.* **100**, 25.

WANG, L. P. & MAXEY, M. R. 1993 Settling velocity and concentration distribution of heavy particles in homogeneous isotropic turbulence. *J. Fluid Mech.* **256**, 27.

YEUNG, P. K. & POPE, S. B. 1988 An algorithm for tracking fluid particles in numerical simulations of homogeneous turbulence. *J. Comput. Phys.* **79**, 373.

YEUNG, P. K. & POPE, S. B. 1989 Lagrangian statistics from direct numerical simulations of isotropic turbulence. *J. Fluid Mech.* **207**, 531.